

# IMAGE PROCESSING ALIGNMENT ALGORITHMS FOR THE OPTICAL THOMSON SCATTERING LASER AT THE NATIONAL IGNITION FACILITY

Abdul A. S. Awwal, Richard R. Leach, Jr., Roger Lowe-Webb, Karl Wilhelmssen,  
Vicki Miller Kamm, Bela Patel, Siddharth Patankar, Tracy Budge

Integrated Computer Control System, National Ignition Facility, Computational Engineering  
Division, Lawrence Livermore National Laboratory, Livermore, CA 94551, USA

## Abstract

Characterizing plasmas generated in the world's largest and most energetic laser facility, the National Ignition Facility (NIF), is an important capability for experimentalists working to achieve fusion ignition in a laboratory setting. The optical Thomson scattering (OTS) laser has been developed to understand the target implosion physics, especially for under-dense plasma conditions. A 5w probe beams can be set up for diagnosing various plasma densities. Just as the NIF laser with 192 laser beams are precisely aligned, the OTS system also requires precision alignment using a series of automated closed loop control steps. CCD images from the OTS laser (OTSL) beams are analyzed using a suite of image processing algorithms. The algorithms provide beam position measurements that are used to control motorized mirrors that steer beams to their defined desired location. In this paper, several alignment algorithms will be discussed with details on how they utilize various types of fiducials such as diffraction rings, contrasting squares and circles, octagons and very faint 5w laser beams.

## INTRODUCTION

The National Ignition Facility (NIF) has made tremendous progress in our understanding of inertial confinement fusion [1]. Recent breakthroughs in fusion performance have attracted worldwide attention to NIF. In NIF, 192 precisely aligned laser beams [2] are designed to irradiate a mm scale fusion target to achieve ignition and produce a net energy gain in a laboratory setting. To achieve this goal, NIF employs several tools to diagnose the plasma condition. The optical Thomson scattering (OTS) laser [3] is such a tool which can deliver a 1 Joule, 5 $\omega$  (211 nm) probe beam with a 1 ns flat-in-time pulse-shape, for diagnosing the plasma temperature at a user-specified time during the plasma evolution in a NIF experiment.

Experiments on NIF can be designed to utilize all 192 or any subset of laser beams. In every case, accurate beam alignment is essential. Beam positions are monitored in the NIF facility using hundreds of CCD cameras distributed throughout each of the 192 beams path. Feedback control loops form the main engine for the NIF automated alignment control system [2]. Position estimates are generated by image analysis algorithms, which are used to align motorized mirror pairs and other optics to direct NIF beams to their desired locations. Starting from the beam source, or Master oscillator, these alignment loops are responsible for

aligning the beams along the complete beam path and finally to the mm size targets located in the target chamber center. In this paper, we will discuss several alignment loops in the OTS laser.

## OTSL ALIGNMENT

A total of eight mirror pairs are closed-loop controlled using more than 14 distinct alignment loops to complete the full alignment of the OTS laser. These alignment points are divided into five main sections as shown in Fig. 1. Starting from the pre-amplifier module (PAM) and through the intermediate amplifier, the beam is taken to the Final Optics Assembly (FOA) via an imaging transport telescope section. The FOA contains frequency conversion crystals to convert the beam to the fifth harmonic and motorized, 5 $\omega$  high-reflecting mirrors to point it to the diagnostic load package (DLP) located in the NIF Target Chamber. Obtaining good OTS data requires precisely overlapping the plasma volume illuminated by the fifth-harmonic probe laser and the plasma-volume imaged by the DLP OTS spectrometer.

The transport vacuum relay telescope (VRT) is used to deliver the conjugate-image of the regen apodization-aperture to the plane of the fifth-harmonic generating crystal; the associated alignment mirror pair ensures the fundamental beam is correctly pointed and centered to the FOA converter line-of-sight for optimum harmonic conversion. Two of the alignment loops discussed here align the ISP laser to the transport telescope input aperture (ISP\_TTI\_PL loop) and the second one aligns the output of the transport telescope to the input of the FOA (OTS\_TTO\_FOA\_PL). Alignment images for both loops are acquired with the same far-field (FF) alignment camera in the FOA but alignment is completed for each loop using different reference fiducials. Specifically, the physical alignment reference for the OTS\_ISP\_TTI\_PL loop is a pair of precision tooling spheres (pinheads) installed in the output optical aperture of the VRT whereas the OTS\_TTO\_FOA\_PL loop is referenced to a commissioned pixel on the FOA FF alignment camera.

2-D and 3-D images for the OTS\_TTO\_FOA\_PL pointing loop are shown in Figure 2. The beam has a dragonfly-shaped appearance with a distinct head and a tail. The coma-like aberrations seen in this image is caused by diffraction since the alignment beam over-fills the aperture of the intermediate amplifier rod and clips on its edge. The alignment feature for this image is the center of the head of the dragonfly-shaped beam. It was determined that a

centroid based algorithm [4] position detection scheme can accurately detect this feature, enabling the VRT output mirrors to be repeatably aligned. The higher brightness of the

head compared to the tail, allows a high-threshold background subtraction-based centroiding, to detect the center of the head of the dragonfly.

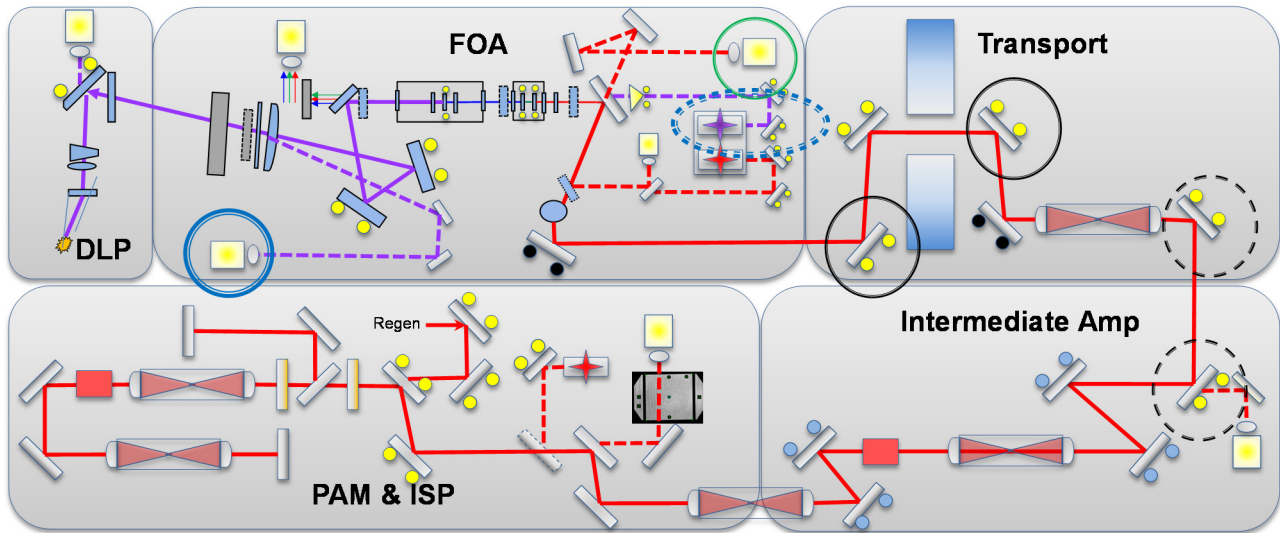


Figure 1: Alignment loops within the OTSL cover 5 sections starting from the Pre-amplifier module (PAM) and Input sensor package (ISP) through the final optics assembly (FOA) which converts the beam to the fifth harmonic and points it to the diagnostic load package (DLP). The mirror-pairs used for the OTS\_ISP\_TTI\_PL are circled with dashed black rings whereas the those used for the OTS\_TTO\_FOA\_PL are solid black rings. Both loops align to the same camera in the FOA circled with a green ring.

Performance of the centroid approach was tested for more than a year and was found to be satisfactory [4]. However, if there is a beam deflection with a magnitude similar to the central spot and period on the order of the image integration time, then the consequent smearing makes the centroid-approach unstable. Consider the cases of motion blur in image 59 and 229 in figure 2, where the position is shifted as the peak is shifted. Comparing the two consecutive images 58 and 59, image 58 shows a single peak with maximum at the head location. The 3-D plot of image 59 shows lowering of the intensity of the head and elevation of the first side lobe of the tail indicative of image smearing. Other images exhibit smearing and displacement in the vertical direction, where multiple heads as well as two tails are visible, as shown in image 91 of Fig. 3.

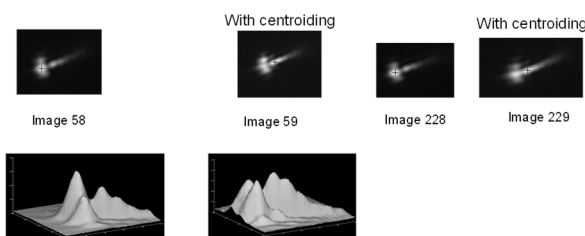


Figure 2: A typical OTSL camera image of OTS\_TTO\_FOA\_PL loop, where OTS is the OTS laser, TTO indicates transport telescope output, (FOA --final optics assembly. PL -- pointing loop). Smearing of images causes a 19 pixel shift in centroid. The surface plot of images 58 and 59 shows the shift of the location of the maximum from the head to the tail.

This weakness in the centroid algorithm prompts us to develop an alternate algorithm.

### Alternate Algorithm to Mitigate Smearing

Matched filtering is well known for its ability to track an object in a complex scene. The dragonfly shape of the OTSL pointing beam makes it a good candidate for using pattern recognition tools based on matched filtering. NIF uses matched filtering techniques [5] to provide robustness and position stability in the presence of illumination gradients, time varying signals, and unpredictable background noise. In comparison, centroid based techniques are affected by all these variables.

To test this approach, we randomly chose a nominal image as a template. Applying the same template to images 59 and 229 resulted in consistent position estimates as shown in Fig. 3. The centroid technique does not produce such a result, as observed above.



Figure 3: The result of matched filtering on the smeared image shows a sensible result.

### Template Selection

When a beam is aligned, the beam may appear initially in any location within the image. To test possible variations, beam image was the shifted from the nominally aligned

Content from this work may be used under the terms of the CC BY 3.0 licence (© 2022). Any distribution of this work must maintain attribution to the author(s), title of the work, publisher, and DOI

position in four directions (left, right, up and down). 100 images were captured in each position. For comparison purposes, we apply the weighted-centroid approach to the sets of images in the nominally aligned position. The result

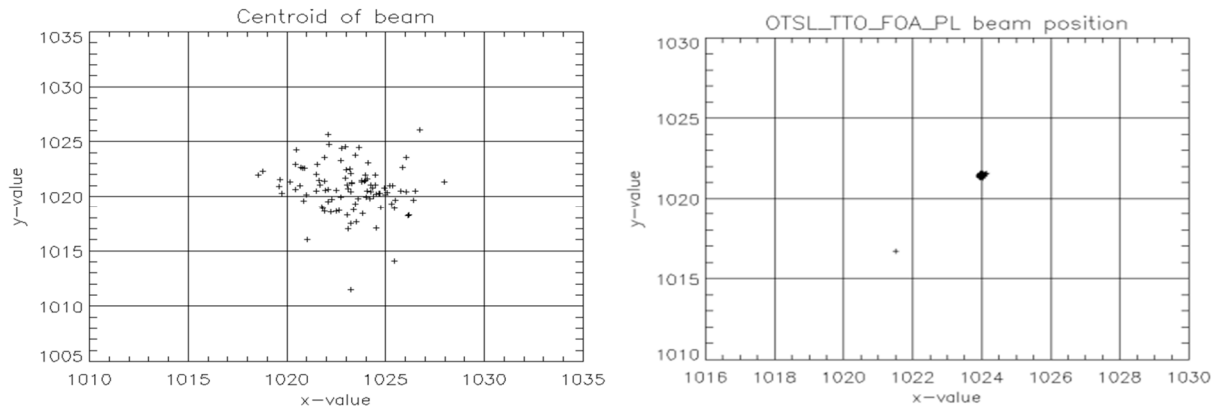


Figure 4: For a 100-image-set of an aligned beam, the scatter plot on the left is generated by the centroid approach where 99% of the spots are within a 7-pixel radius. The scatter plot on the right is generated with a template (image65). The 99% encompassing radius is reduced to a tight cluster with a span of 0.3 pixels.

Variations in intensity within the head of the dragonfly image, from image to image, produces variations in the centroid based beam position estimate.

Moving the position of the beam can cause the shape to change. However, in practice, the measurement will be for a consistent spot when it is in the fixed aligned position, for that reason the align65 template was deployed. Next, we look at the second OTSL alignment loop.

### ALIGNING DIFFRACTION RING

Alignment fiducials in the beam image are often used to help locate the beam or reference position. One of the OTSL alignment loops, ISP\_TTI\_PL, uses out of focus imaging of a spherical object connected to a shaft as a fiducial. These fiducials are positioned at the edge of the optical aperture of the circularly formatted alignment laser beam. The alignment camera is focused to image the NF relay plane which is about 40 meters away from the pointing reference fiducials. The beam leading to a clipped diffraction pattern. The out-of-focus imaging produces a pair of diffraction rings at the top and bottom of the alignment image as shown in Figure 5. Both rings are present with partially missing portion. The objective of this alignment algorithm is to detect the center of the diffraction rings under various imaging conditions.

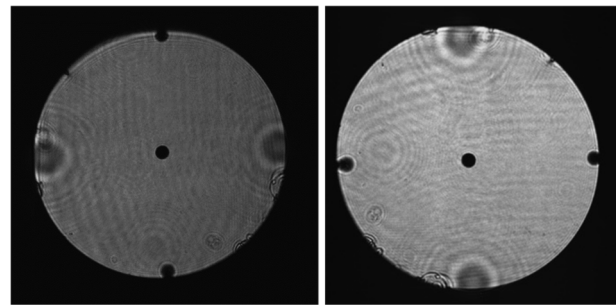


Figure 5: (a) A typical OTSL camera image ISP\_TTI\_PL loop, where ISP is the ISP laser, TTI indicates transport telescope input, and PL stands for pointing loop. Every beam is aligned using a pointing and centering move (b) The diffraction rings may appear in the top and bottom, note that the left ring was moved to the top.

### Algorithm

The diffraction rings intensity levels are very similar to the background making a threshold-based approach centroid approach not possible for meeting alignment requirements. Since the diffraction ring has a distinct pattern however, pattern recognition techniques based on matched filtering [5] is a viable option. As a first approximation, the template is considered to be a circular ring, with a fraction missing to resemble the missing part of the diffraction as shown in Fig. 6. The parameters inner radius,  $r\_est\_left$ , ring thickness,  $\delta$ , percentage of the ring missing from one side, missing fraction defines the template. If missing fraction is 50% then half of the ring is missing.

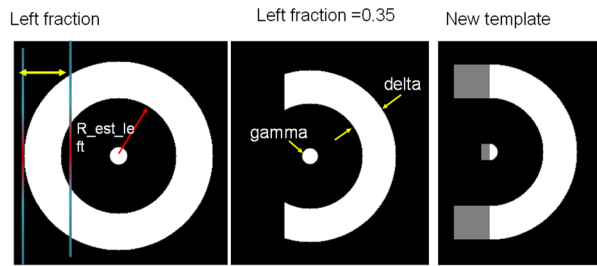


Figure 6: The template showing 4 parameters defining it: estimated radius for left ( $R_{est\_left}$ ), radius of inner spot ( $\gamma$ ), width of the ring ( $\delta$ ) and missing fraction (left fraction). The new template design instead of a full circular ring use half circle with linear extension (on the right).

To avoid spurious correlation peaks, two rings are initially segmented using the angular location from a global centroid [6]. During alignment, the missing fraction for both rings changes. It was found that if the missing fraction of both rings remained same, the template in Fig. 6 performed well, however, as the image moved in four directions the template was unable to detect the center accurately. To correct an incorrect position using angular position and distance, one must be certain which of the two position is correct.

### Certainty Detector

As inspired by a bipolar binary associative memory [7] single computational neuron, is used to evaluate the quality of the location detected. The function of the neuron is to generate a high score when there is a match of the stored pattern with the input pattern and a low score when there is no match. Here the stored pattern is the cross-section of the template in bipolar binary. When the position is correct, high score of above 80 is obtained. For a totally incorrect position, the score is highly negative. These scores are used to generate the uncertainty of the position as well as correct an incorrect position.

### Template Design II

A simulation of the Nfiducial diffraction pattern reveals that the ideal diffraction pattern may not actually contain a complete circular ring, rather it is partially circular and partly linear. Therefore, the template was redesigned as depicted in the right side of Fig. 6, where a half circular ring is extended by the straight edge of the template in a linear fashion up to an extent defined by the missing fraction. The weight of the linear extension was 50% compared to the weight of the right half, to reduce the effect of the high intensity near the edges which has biased the previous centering position.

### Optimization

During alignment, the rings do move relative to the large disc, and as such the rings appear with different missing fraction as shown in Fig. 7. To capture the possible variations of the alignment images, the nominally aligned position image (used in Phase I) was moved in four directions

to the left, right, up, and down and 100 images were captured in each position. One image from the set is shown in Fig. 7.

To choose the optimized parameters defining the template, the position detection program is executed in a loop with varying four parameters: inner radius, width of the ring, radius of the inner disc, and missing fraction on single image for both left and right rings in the aligned set of 100 images. Solution which gives minimum divergence of each position in terms of standard deviation is chosen after visual verification. Then process of stability check is then applied to the remaining 400 image sets at all the other positions above. After that the solution is applied to a data set taken from the images archived in the NIF for the previous 6 months. Using this data set, a variety of templates was applied until a solution was found that worked robustly on the entire set of NIF images.

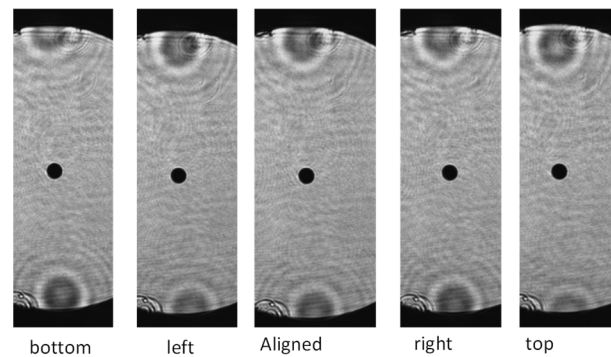


Figure 7: The variation of the diffraction rings as it moves left right and up and down with respect to the aligned position.

Figure 8 shows the difference between templates I and II design. The left results show, the phase I template introduce bias in the lower position. In phase II, the result is improved significantly with lower incidence of bias towards any specific direction as shown in the right onset.

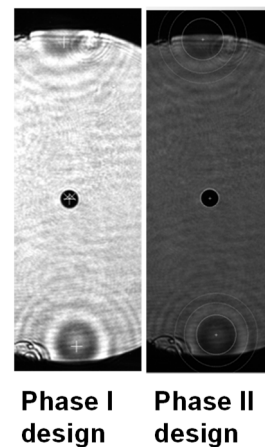


Figure 8: The variation of the diffraction rings as it moves left right and up and down with respect to the aligned position.

Content from this work may be used under the terms of the CC BY 3.0 licence (© 2022). Any distribution of this work must maintain attribution to the author(s), title of the work, publisher, and DOI

The optimized parameters are, top template radius = 77, width = 48, missing fraction = 0.3 and gamma = 12 and the bottom template radius = 73 width = 45, missing fraction = 0.6 and gamma = 12. After position estimation, the missing fraction is re-calculated. If the supplied missing fraction was very different from the re-estimation of the same, and it also had a negative score, only then was the algorithm allowed to recalculate the predicted second spot. Most of the time, the new missing fraction calculated online was used to stop predicting the second spot and avoid oscillation, which could make the alignment in a closed loop very difficult. Correlation-based approaches must be guarded against spurious detection. After the two rings are located, the position data obtained is subjected to several spacing tests. Such spacing tests with certain tolerance help us to eliminate spurious spots from the solution.

Next, we look at an alignment loop algorithm for centering the OTSL 5w laser.

### OTSL SQUARE BEAM ALIGNMENT

One of the more challenging image processing loops in OTSL is the AA\_OTSL\_PILOT\_CL loop. The image processing algorithm for this loop uses multiple, superimposed image features to locate the beam reference and the beam center to enable proper laser alignment. The features consist of parallel opposing beam edges (reference location) and parallel opposing lines or dark bands (beam location) to estimate the 5w beam centering offsets. The images for this loop tend to have high noise within the image as well as near desired beam edge features. In addition, image illumination is often poor and can have undesired gradients near the beam edges. A typical image example is shown in Fig. 9.

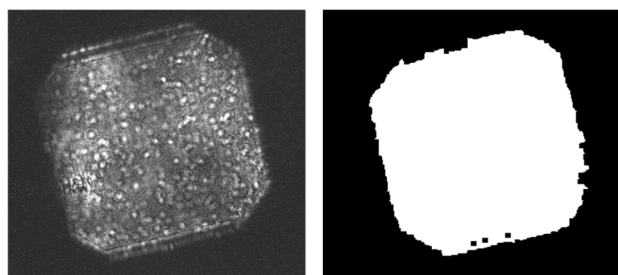


Figure 9: A typical OTSL 5w camera image for the AA\_OTSL\_PILOT\_CL loop (left). The Crosshairs algorithm is used to determine the left and right parallel opposing edges as well as the top and bottom parallel opposing lines or dark bands in the image. The center of the line and edge positions are returned as the beam and reference center locations. The output mask of the adaptive beam location algorithm is shown on the right.

The beam edges and reference lines are found initially using the adaptive beam location algorithm and then further refined with the crosshairs algorithm. The crosshairs algorithm has been used with great success in many loops in the NIF automated alignment control system [8-10]. Crosshairs has proven to be tolerant to object rotations, noise, changes in illumination and target object properties such as line thickness.

All images initially undergo a process to quickly identify unacceptable or ‘off-normal’ images. The off-normal processor is an image analysis routine that contains a suite of selectable tests each of which analyze the image and classify it as a good or bad image. The tests are limited to basic or common image errors such as an image that is unacceptably dim or blank, missing the beam, all-white, etc.

### Adaptive Beam Estimator Algorithm

After successful off-normal processing, an initial beam location estimate mask is found with the adaptive beam location algorithm. This algorithm employs an iterative intensity level process to create an optimize mask for the desired image object(s) [11]. To begin, the image is filtered with a non-linear edge preserving filter[12]. All objects at each intensity level are identified and tested for a set of criteria, for example: size, ranging, signal to noise of objects found, and object location in the image.

The resulting mask created is seen in Fig. 9. The edges of the mask are used to identify the initial, general locations of the beam and reference features. The edges are used to identify sub-image areas to locate initial reference lines or beam edge locations. Sub-image boundaries can be seen outlined in green in the lower right plot in Fig. 10.

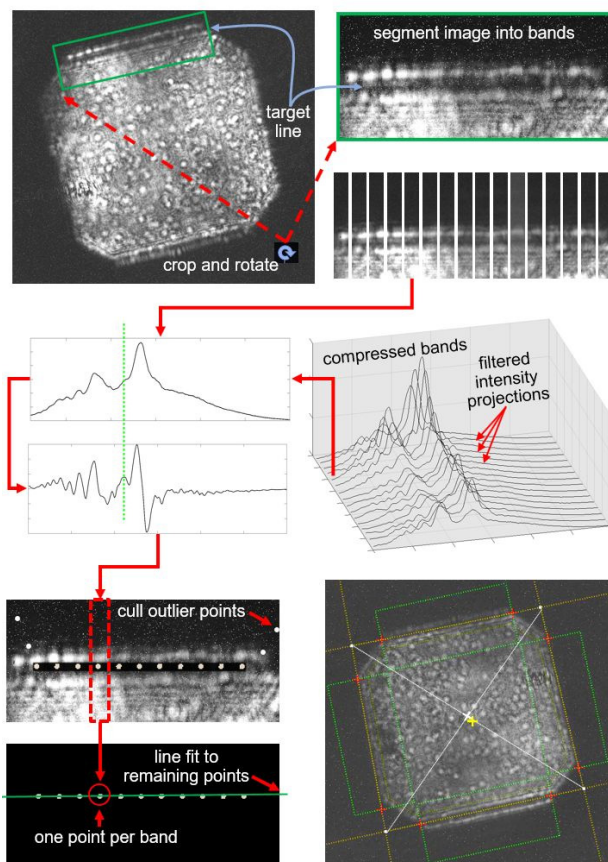


Figure 10: Crosshairs is executed by first rotating the sub-image to orient the target line or edge (top). The image is then segmented into orthogonal slices or ‘detection bands’ (lower top right). The bands are transformed into a set of intensity vectors by calculating the mean projection for each band (middle). The intensity vectors are then

processed and filtered individually to identify the edge or line center location for that band (middle left). This results in a set of points, one point per band (bottom left). A series of tests on the resulting set of points is performed to remove outliers. Finally, a least squares linear fit of the remaining points is used to determine the optimal target feature fit (green lines). Final beam location is seen as the yellow + and the reference as the white x and are used to guide beam alignment.

### Crosshairs Algorithm

Resulting edge and line locations are then processed and refined with the crosshairs algorithm. A diagram of an example of the complete crosshairs process is illustrated in Fig. 10. Crosshairs is executed by first rotating the sub-image to orient the target line or edge. The image is then segmented into orthogonal slices or 'detection bands'. The bands are transformed into a set of intensity vectors by calculating the mean projection for each band. The intensity vectors are then processed and filtered individually to identify the edge or line center location for that band. This results in a set of points, one point per band. A series of tests on the resulting set of points is performed to remove outliers. Finally, a least squares linear fit of the remaining points is used to determine the optimal target feature fit. Uncertainty for any given line estimate is calculated and reported using the mean deviation of the points used in the line fit. The uncertainty is used to abort the alignment if the deviation does not meet the loop requirements. Final beam and reference locations can be seen in Fig. 10 as the yellow + and the reference as the white x and are used to guide beam alignment. Optics adjustments are made until they are co-located and thus alignment for the AA\_OTSL\_PILOT\_CL loop is complete.

### CONCLUSION

This paper describes the image processing associated with several OTSL alignment loops. In the first two examples, template-based matched-filtering approach was utilized. The last algorithm uses an adaptive beam location algorithm and then is further refined with the crosshairs algorithm.

### ACKNOWLEDGEMENTS

\*This work was performed under the auspices of the U.S. Department of Energy by Lawrence Livermore National Laboratory under Contract DE-AC52-07NA27344. This paper is released as LLNL-CONF-827599-DRAFT. The author wishes to acknowledge the help from Alexandra Saabye for helping with the review and release process.

### REFERENCES

- [1] A. L. Kritcher, A. B. Zylstra, D. A. Callahan, O. A. Hurricane, *et al.*, "Achieving record hot spot energies with large HDC implosions on NIF in HYBRID-E," *Phys. Plasmas* 28, 072706, 2021, doi: 10.1063/5.0047841
- [2] S. C. Burkhart, E. Bliss, P. Di Nicola, D. Kalantar, R. Lowe-Webb, *et al.*, "National Ignition Facility System Alignment", *Applied Optics*, Vol. 50, Issue 8, pp. 1136-1157 (2011)
- [3] J. Galbraith, P. Datte, S. Ross, G. Swadling, S. Manuel, B. Molander, B. Hatch, D. Manha, M. Vitalich, B. Petre, "Design of an Optical Thomson Scattering diagnostic at the National Ignition Facility," *Proc. SPIE 9966, Target Diagnostics Physics and Engineering for Inertial Confinement Fusion V*, 99660E, 2016.
- [4] A. Awwal, "Alignment of pointing beam in the Optical Thomson Scattering Laser at the National Ignition Facility," *SPIE Proc. 11841, Optics and Photonics for Information Processing XV*; 118410I (2021), doi.org/10.1117/12.2596187
- [5] A. A.S. Awwal, E. Bliss, G. Brunton, V. Miller, R. R. Leach, V. Miller, R. Lowe-Webb, R. Roberts, and K. Wilhelmsen, "Centroid stabilization for laser alignment to corner cubes: designing a matched filter," *Applied Optics*, Vol. 56(1), pp. A41-A51, 2017.
- [6] A. Awwal, "Alignment of diffraction features in the Optical Thomson Scattering Laser at the National Ignition Facility," *SPIE Proc. 11666, High Power Lasers for Fusion Research VI*; 116660D (2021) doi.org/10.1117/12.2588507
- [7] A. A. S. Awwal, M. A. Karim, and H. K. Liu, "Machine Parts Recognition Using a Trinary Associative Memory," *Optical Engineering*, Vol. 28, pp. 537-543, 1989.
- [8] R. R. Leach Jr., A. Awwal, E. Bliss, R. Roberts, M. Rushford, K. Wilhelmsen, and T. Zobrist, "Analysis of the confluence of three patterns using the Centering and Pointing System (CAPS) images for the Advanced Radiographic Capability (ARC) at the National Ignition Facility," *Proc. SPIE 9216, Optics and Photonics for Information Processing VIII*, 92161Q (14 October 2014).
- [9] R. R. Leach Jr., A. A. S. Awwal, S. J. Cohen, R. R. Lowe-Webb, R. S. Roberts, J. T. Salmon, D. A. Smauley, K. Wilhelmsen, "Alignment mask design and image processing for the Advanced Radiographic Capability (ARC) at the National Ignition Facility," *SPIE Proc. 9598*, 959819 (2015).
- [10] R. R. Leach Jr., A. A. S. Awwal, R. Lowe-Webb, V. Miller-Kamm, C. Orth, R. Roberts, K. Wilhelmsen, "Image processing for the Advanced Radiographic Capability (ARC) at the National Ignition Facility," *Proc. SPIE 9970, Optics and Photonics for Information Processing X*, 99700M (14 September 2016).
- [11] A. A. S. Awwal, R. R. Leach Jr., "Image processing strategies and multiple paths toward solutions," *Proc. SPIE 10751, Optics and Photonics for Information Processing XII*, 107510R (7 September 2018).
- [12] M. Kuwahara, K. Hachimura, S. Eiho, M. Kinoshita, "Digital Processing of Biomedical Images," Plenum Press, pp. 187-203, New York, NY, 1976.